

Nondestructive inspection of luxury yacht glass reinforced composite panels by means of transient thermography

by R. Montanini* and F. Freni*

* *Department of Industrial Chemistry and Materials Engineering, University of Messina, C.da di Dio, San'Agata di Messina, I-98166, Italy, rmontanini@ingegneria.unime.it, ffreni@ingegneria.unime.it*

Abstract

Active thermography measurement techniques, based on modulated optical excitation with either reflection or transmission set-up, have been implemented for quantitative assessment of simulated subsurface defects in thick glass reinforced composite laminates employed for luxury yachts construction.

The paper investigates detection limits associated to defect's size, shape and depth as well as recognition of small impact damages over the external gel-coat finishing layer. The obtained results demonstrated the effectiveness of thermal NDE as a powerful and non contact measurement tool for the inspection of large GFRP structures. In particular, results showed that optical lock-in thermography method allows accurate estimation of impact damages (percentage error < 1%), whereas the accuracy of delamination detection and sizing is critically influenced by both defect's area and shape ratio (l/h), because of multi-dimensional diffusion phenomena.

1. Introduction

Since 80's composite materials started to have a fundamental role in the construction of small boats and luxury yachts, owing to their significant benefits in terms of light weight, fatigue and corrosion resistance and aptitude to be modeled in complex shapes. The widespread use of glass reinforced composites (GFRP) in nautical applications requires suitable nondestructive evaluation (NDE) techniques able to address structural safety and quality issues which are of primary concern for customers [1]. Well-known NDE methods, such as ultrasonic C-scans and x-ray radiography, are rather difficult to be implemented in the boatyard environment [2]. Hence, there is an increasing interest in the development of new NDE methods allowing the inspection of large hull structures in a fast and reliable way. Among these, active thermography (either transient or modulated) is one of the most promising one, since it allows fast examination of large surfaces with good sensitivity and it is already routinely employed in other fields, e.g. aerospace.

The active approach involves using an excitation source to induce thermal contrast into the material and an IR camera to measure the stationary or transient response. Pulsed thermography (PT), in which the specimen is heated for few seconds and the thermal decay response at the surface is measured by the infrared camera, is one of the most common thermal stimulation method [3-6]. Subsurface defects will partially reflect or stop heat flows, producing hot spots (in a reflection set-up) or cold spots (in a transmission set-up) on the analysed specimen surface. Defects detectability strongly depends on the temperature contrast between the defected area and the sound area of the material, which is related to defects features like depth, extension and orientation. Lock-in thermography [7-16] makes use of modulated optical stimulation to heat the sample, whose thermal emission in the infrared range is remotely detected by the IR camera. The term lock-in refers to the necessity of monitoring the exact time dependence between the output signal and the reference input signal (i.e., the modulated heating). Hence, amplitude and phase images of the reconstructed thermal wave can be computed for each heat-generating frequency using the Fourier transform algorithm. A measurement technique which combines the advantages of both lock-in and pulse thermography without sharing their drawbacks is pulse phase thermography, which has been first proposed by Maldague and Marinetti [17-18]. The specimen is pulse heated as in pulsed thermography and the mix of frequencies of the thermal waves launched into the specimen is unscrambled by computing the Fourier transform of the temperature evolution over the field of view; the phase, or magnitude, image can be presented as in modulated lock-in thermography.

Most of the research in this field has addressed some important issues but many questions still remains open when dealing with the technological transfer to an industrial application.

This study aims to explore the implementation of lock-in thermography as an effective tool for the nondestructive evaluation of delamination and impact defects in thick glass-reinforced composite laminates used in luxury yachts hull structures.

2. Material and methods

2.1 Specimens preparation

Experimental tests were carried out on three glass fibre reinforced polymer (GFRP) panels of thickness (s) equal to 9 mm, which were provided by a luxury yachts shipyard (Abacus Marine Spa, Giammoro, Messina, Italy). The laminates were layed-up manually with six layers of glass fibre (800/300 g/m²) embedded in polyester resin. Within two of these panels, namely type 1 and type 2, artificial defects, simulating a delamination discontinuity, were inserted by placing polytetrafluoroethylene (PTFE) thin films ($t=0.2$ mm) between successive layers during the lamination.

A schematization of the realized defected panels is shown in figure 1.

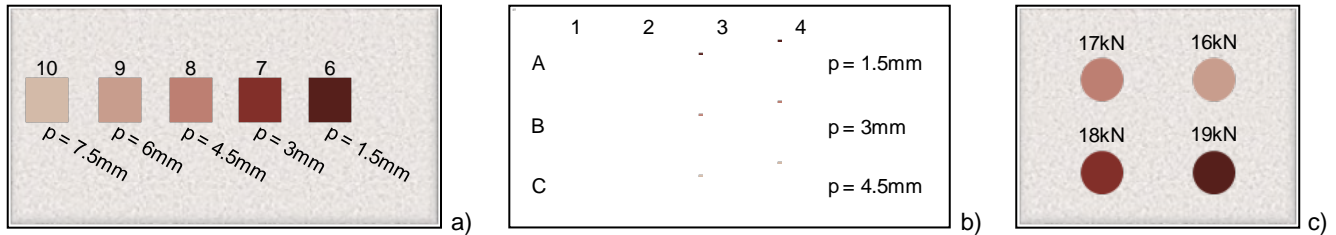


Fig. 1. Schematization of GFRP reference panels; a) panel type 1, with five equal defects placed at different depth; b) panel type 2, with four different shaped defect placed in three rows at different depth; c) panel used for impact defect size evaluation with four circular damaged areas obtained with increasing compression loads

The type 1 sample panel (figure 1a) was used to verify the possibility of esteeming flaws location. Five equal square inclusion (characteristic width 10 mm), placed at different depth (p), from 1.5 mm to 7.5 mm, with steps of 1.5 mm, were manufactured.

The type 2 sample panel (figure 1b), instead, was exploited to explain the influence of the defect's aspect ratio. For this reason four different shaped PTFE layers, with same characteristic dimension (circle with $d=10$ mm, equilateral triangle with $l=10$ mm, rectangle with $l=10$ mm and $h=5$ mm, square with $l=10$ mm), were placed at three different depths, starting with 1.5 mm up to 4.5 mm.

A third specimen (figure 1c) was manufactured to study the possibility of estimating areas of surface impact damages. This panel is similar to the other ones, but it has a different superficial finishing, because a hard and smooth gel coat layer had been applied, as usually done in nautical applications in order to increase the surface hardness and protect the material from humidity. Four impact defects were simulated by means of a material testing machine, equipped with a spherical head ($d=27$ mm) steel punch, using increasing compressive loads from 16 kN to 19 kN, with 1kN incremental steps.

2.2 Measurement techniques

The experimental tests have been carried out using a FLIR Titanium 560 M camera, with a 640 x 512 pixels InSb focal plane array detector, working in the MWIR (3.6 – 5.1 μ m) spectral band (NETD < 20 mK at ambient temperature).

Tests were performed using optical lock-in thermography (OLT), with an excitation source consisting of five halogen lamps (long pulse > 500 ms) of 1 kW power each. Hence, thermal waves are launched into the specimen and the resulting temperature field of its surface is measured in the stationary regime. The acquisition of four equidistant points $S_i(x,y)$, recorded over the sample surface during each modulation period, permits to evaluate the discrete one-dimensional Fourier transform (DFT) on each pixel of the thermogram, calculate the real and imaginary parts and, finally, the amplitude $A(x,y)$ and phase $\Phi(x,y)$ images:

$$A(x,y) = \sqrt{[S_1(x,y) - S_3(x,y)]^2 + [S_2(x,y) - S_4(x,y)]^2} \quad (1)$$

$$\Phi(x,y) = \tan^{-1} \left[\frac{S_1(x,y) - S_3(x,y)}{S_2(x,y) - S_4(x,y)} \right] \quad (2)$$

Both amplitude and phase images were used to evaluate the presence of defects, but the latter offers many advantages respect to the other one, because of its insensitivity to non homogenous surface emissivity or thermal excitation.

The OLT test method was setup in reflection mode for the evaluation of defect's depth (sample panels type 1-2) and shape ratio sensitivity, whereas either reflection or transmission setup were used to assess impact damages. The experimental setup is shown in figure 2.

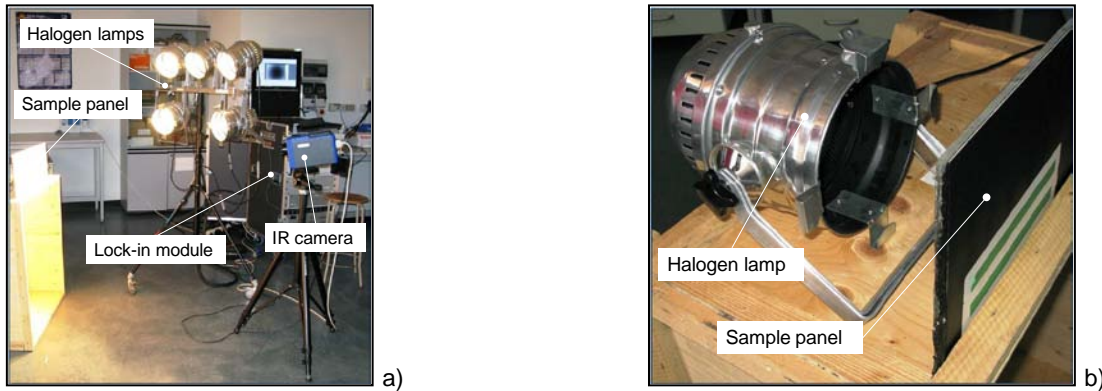


Fig. 2. Experimental setup for OLT measurements on GFRP sample panels: a) reflection mode, b) transmission mode .

In reflection setup (figure 2a) the IR camera and the excitation source (i.e. halogen lamps) were positioned on the same side with respect to the sample, whereas in transmission mode (figure 2b) the sample was interposed between the IR camera and the excitation source (only one lamp, 1 kW power).

3. Experimental results

3.1. Estimation of delamination defects and aspect ratio influence

Several tests were carried out on the type 1 sample panel in order to investigate the possibility of estimate defects depths, by analyzing phase trends as a function of the lock-in frequency. A normalized standard contrast was defined as follows:

$$C^n(t_f) = \frac{\Delta\Phi(t_f)}{\Phi_s(t_f)} = \frac{\Phi_{def}(t_f) - \Phi_s(t_f)}{\Phi_s(t_f)} \quad (3)$$

where $\Phi_{def}(t_f)$ and $\Phi_s(t_f)$ are the average phase values of defected and surrounding areas, evaluated at the end time t_f of the test. This function permits to calculate a frequency of first apparition, as the one at which normalized contrast reaches a defined threshold; this value of frequency permits to get an estimation of flaw depth, as follows:

$$C^n(t_f) = C^t \quad \rho = 1.8 \sqrt{\frac{\alpha}{\pi f}} \quad (4)$$

where $C^n(t_f)$ is the normalized standard contrast evaluated at the end of test, C^t is the threshold value of contrast, α the thermal diffusivity of GFRP, f is the lock-in frequency.

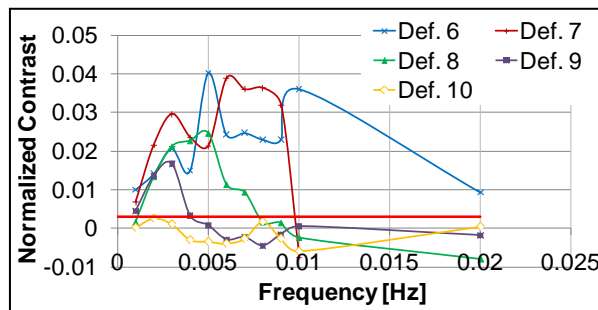


Fig. 3. Contrast trends as a function of the lock-in frequency for defects number 6 ($p=1.5$ mm), 7 ($p=3$ mm), 8 ($p=4.5$ mm), 9 ($p=6$ mm) and 10 ($p=7.5$ mm). Red line shows the threshold level used, in this case equal to 0.003.

In figure 3 the impact of the lock-in excitation frequency on the normalized standard contrast is illustrated. As expected, for each defect the contrast reaches a maximum value for frequencies linked to its specific depth. In fact, the first

defect that appears by decreasing the lock-in frequency is defect 6 ($p=1.5\text{mm}$), followed by the others, in order of nominal depths. Even using very low frequencies (0.001 Hz), the deepest defect (10) was never detected.

Figure 4 shows defect visualization on type 1 panel for different lock-in frequencies.

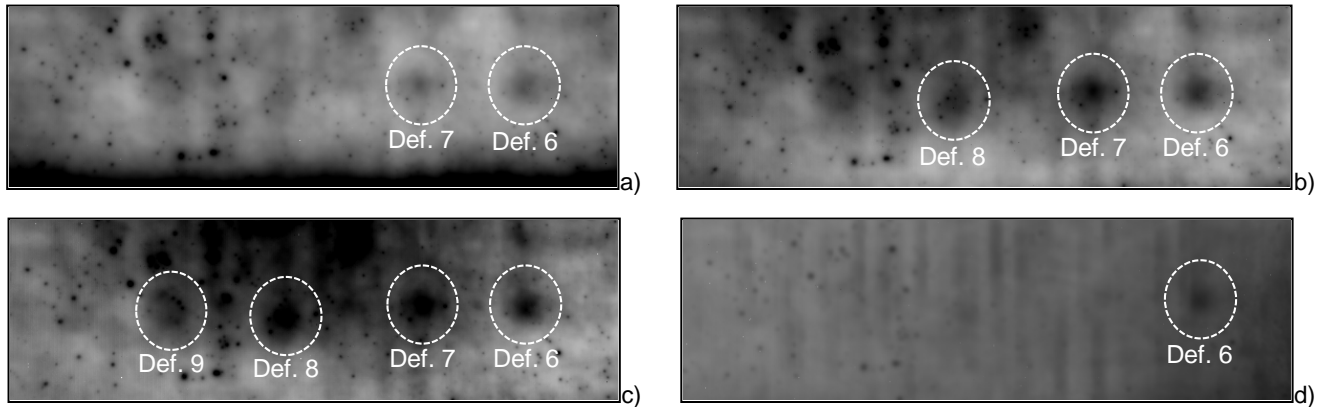



Fig. 4. Grey level phase image of panel type 1 (def. 6-7-8-9-10) obtained by OLT in reflection mode with heat power amplitude of 50%: a) $f_{lock-in} = 0.001$ Hz; b) $f_{lock-in} = 0.002$ Hz; c) $f_{lock-in} = 0.004$ Hz; d) $f_{lock-in} = 0.01$ Hz

For frequencies higher than 0.01 Hz all defects but defect 6 were not detected. The reduction of the lock-in frequency leads to a good visualization of defects, except for defect 10 ($p=7.5$ mm), that was never “seen”, because of its too small surface area. Hence, the actual defect’s reflecting area is a very important parameter for detectivity, for the reason that during a lock-in test in-plane thermal diffusion is involved, causing a strong reduction of the thermal contrast between defected and surrounding areas. This effect increases for long test durations and leads to the impossibility of detecting discontinuities with small thermal reflecting area at lower frequencies (0.001 Hz = 1000 s).

In Table 1 defects characteristics, nominal depths, experimental depths and percent error are summarized.

	Characteristic dimension [mm]	Defect area [mm ²]	Defect ID	Nominal depth [mm]	First apparition frequency [Hz]	Estimated depth [mm]	Error [%]
	l = 10	100	6	1.5	0.0223	1.93	28.79
			7	3	0.0097	3.10	2.97
			8	4.5	0.0078	3.44	-23.48
			9	6	0.0040	4.76	-20.66
			10	7.5	-	-	-

Tab. 1. Characteristic of artificial delaminations in GFRP panel 1 ($s=9$ mm) and experimental results for depth estimation. Test method: lock-in thermography in reflection set-up.

Significant percentage errors (up to 29%) were found between estimated and nominal defect’s depth. One possible explanation for this discrepancy might be due to the very low lock-in frequencies required to detect the defects embedded in the GFRP panel, which in turn depends on the actual thermal wave flow established within the material. Tests performed by increasing the number of modulation cycles did not improve detectability as well. In contrast to CFRP used in aerospace structures, nondestructive testing of glass-reinforced composites by means of OLT seems to be more troublesome, probably because of the high transmittance in the MWIR range of GFRP. This aspect actually could represent a severe limit for the inspection of thick laminates, as those tested in this work.

The influence of defects shape ratio was investigated by means of the test panel type 2, using a lock-in setup in reflection, with modulation frequencies comprised in the interval from 0.001 Hz to 0.04 Hz.

Figure 5 shows normalized standard contrast trends as a function of the lock-in frequency for defects of type A ($p=1.5$ mm). The contrast plot shows the same trend for each defect, with a sharp increase at very low frequencies, a maximum value for $f = 0.004$ - 0.006 Hz, followed by a progressive decrease as the lock-in frequency is raised up. For frequencies higher than 0.025 Hz, none of the defects was detected. Similar trends were found for defects of type B and C.

Phase thermograms are shown in figure 6.

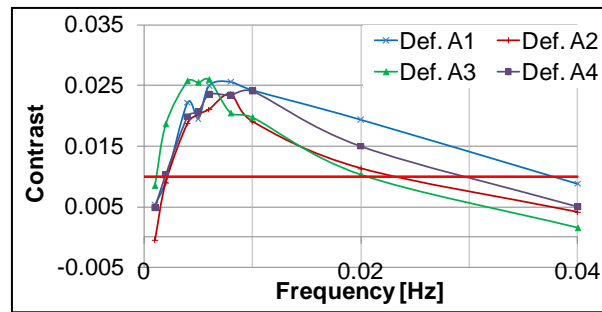


Fig. 5. Contrast trends as a function of lock-in frequency for defects type A: A1 (circle with $d=10$ mm), A2 (triangle with $l=10$ mm), A3 (rectangle with $l=10$ mm), A4 (square with $l=10$ mm). Red line shows the threshold level used, equal to 0.01.

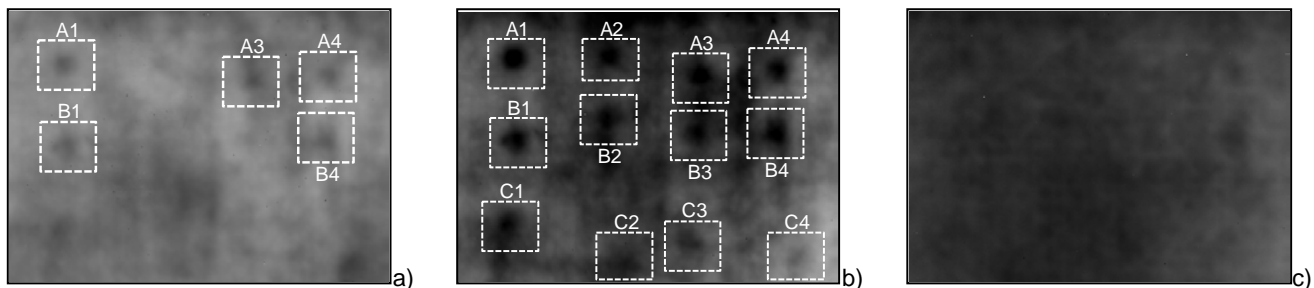






Fig. 6. Gray level phase image of panel type 2 (def. A-B-C) obtained by OLT in reflection mode with heat power amplitude of 50%: a) $f_{lock-in} = 0.001$ Hz; b) $f_{lock-in} = 0.005$ Hz; c) $f_{lock-in} = 0.04$ Hz.

The obtained results are illustrated in table 2. For each of the three rows, the same sequence of first appearing frequency was noted: circular one (1), followed by squared (4), triangular (2) and rectangular (3). The main differences between the defects were the aspect ratio and the area. By introducing the aspect ratio h/l , a good correlation between this parameter and defects detectability can be highlighted. It is interesting to observe that, by comparing the square and circular defects (that are characterized by the same h/l aspect ratio) it seems that the absence of sharp edges leads to an easier defect detection. In contrast, the actual area does not seem to have a direct correlation, although the two discontinuities that are first detected are also those having the largest area.

	Characteristic dimension [mm]	Defect area [mm ²]	Defect ID	Nominal depth [mm]	First apparition frequency [Hz]	Estimated depth [mm]	Error [%]
	d = 10	78.5	A1	1.5	0.0376	1.57	4.77
			B1	3	0.0123	2.74	-8.40
			C1	4.5	0.0055	4.10	-8.69
	l = 10 h/l=0.866	43.3	A2	1.5	0.0228	2.02	34.54
			B2	3	0.008	3.40	13.57
			C2	4.5	0.005	4.10	-4.23
	l = 10 h = 5 h/l = 0.5	50	A3	1.5	0.0203	2.14	42.59
			B3	3	0.0074	3.54	18.08
			C3	4.5	0.0046	4.49	-0.15
	l = 10 h/l = 1	100	A4	1.5	0.0293	1.78	18.68
			B4	3	0.0108	2.93	-2.25
			C4	4.5	0.0052	4.23	-6.09

Tab. 2. Characteristic of artificial delaminations in GFRP panel 2 ($s=9$ mm) and experimental results for depth estimation. Test method: lock-in thermography in reflection set-up.

The obtained results highlight the importance of the aspect ratio in defect detection, although further investigations are needed.

3.2. Estimation of impact damages on gel-coat surface

The aim of this experimental section was to analyze the possibility of dimensioning simulated surface impact defects using phase image obtained by OLT method. In this case, both reflection and transmission modes have been investigated.

The estimation of discontinuities diameter was carried out by analyzing phase trends along a linear profile intersecting the maximum diameter of each defect. Phase images are shown in figure 7.

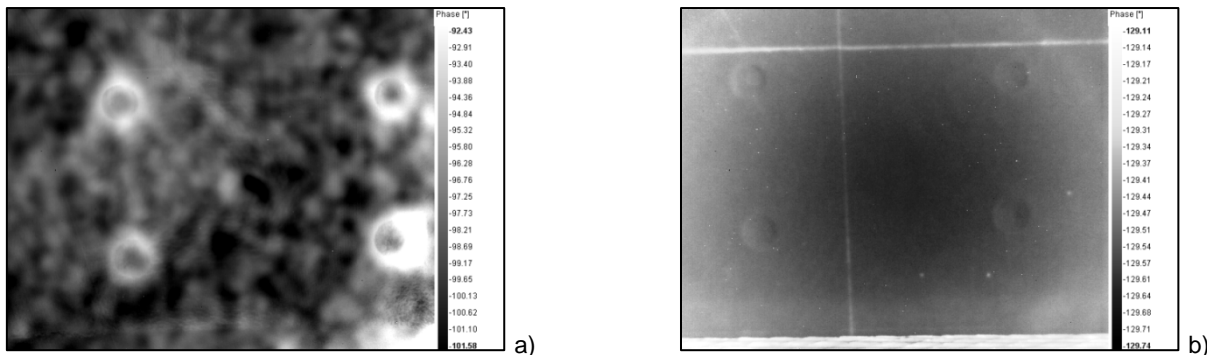


Fig. 7. Impact damage evaluation: a) grey level phase thermogram obtained by OLT in transmission mode ($f_{lock-in} = 0.05\text{Hz}$, Amplitude = 80%); b) grey level phase thermogram obtained by OLT in reflection mode ($f_{lock-in} = 0.5\text{Hz}$, Amplitude = 80%)

In the transmission mode, the presence of surface defects results in a local alteration of the thermal flow, causing a marked phase gradient with respect to the surrounding area, as can be seen in figure 8. In this figure it's possible to analyze the phase trend as a function of the distance, along four linear profiles traced intersecting one defect each. It's possible to note that phase shows a substantial increase in correspondence to the damage area edges. Sizing of the damaged area can then be easily carried out by calculating the distance between the two higher peaks. More severe impacts lead to higher phase differences. In addition, phase gradients are much more consistent than in the reflection mode (cnf. Figure 7a and 7b).

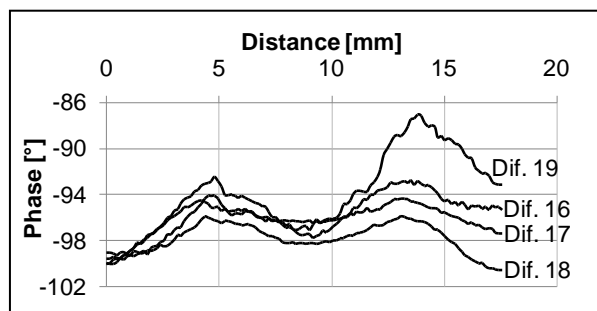


Fig. 8. Phase trends as a function of the distance calculated along four linear profiles intersecting maximum diameter of each defect, obtained by lock-in thermography in transmission mode

In reflection mode, although defects are well contrasted with respect to the sound area, the phase difference is much less sharp (figure 7b). Moreover, defects sizing is sometimes more troublesome. Defects located less favourably with respect to the heating source seem to manifest a different behaviour in the phase plot, as can be seen in figure 9 by comparing defects 16-19 (actually nearer to the heating source) and 17-18.

In the latter case, depending on the heating direction, either a sharper increase or a reduction of the phase angle is clearly observed, because lamps were not positioned head-on to the sample surface but they were slightly decentralized. This results in thermal waves in-plane (from right to left on the panel) diffusion, that, in presence of a discontinuity, is affected by a "shadowing effect" due to defect surfaces positioned on the same part of the lamps (right side of flaw), and in a "gaining effect" on the opposite side. Diameters of defects were estimated calculating the distance between the two peaks (positive and negative) in the phase angle plot.

The second case (def. 16-19) shows an increase of the phase for both damages, and maximum values are not marked as in the previous case. This might be due to the fact that those two defects are closer to the lamps, so their shadowing and gaining effects are not visible as for other defects.

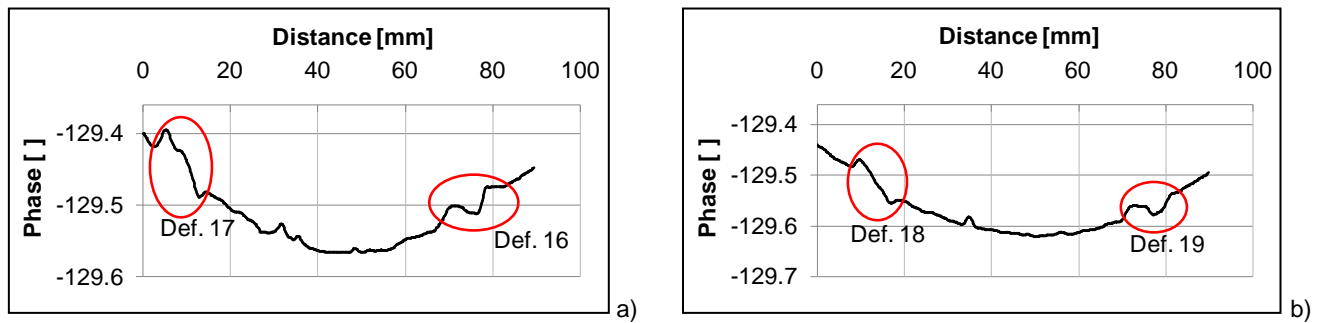


Fig. 9. Phase trends as a function of distance, following two linear profiles intersecting maximum diameter of each defect, obtained by lock-in thermography in reflection mode; a) defects 17-16; b) defects 18-19.

Nominal dimensions, estimation and percentage error are presented in table 3.

	Def. 16	Def. 17	Def. 18	Def. 19
Nominal diameter [mm]	8.30	8.50	8.65	8.90
Estimated diameter [mm]	8.41	8.56	8.71	9.01
% error	1.34	1.32	1.30	1.26

	Def. 16	Def. 17	Def. 18	Def. 19
Nominal diameter [mm]	8.30	8.50	8.65	8.90
Estimated diameter [mm]	7.22	7.88	8.05	7.88
% error	-12.9	-6.67	-6.39	-11.39

Tab. 3. Nominal dimensions, estimations and % error for def. 16-17-18-19, left) obtained by transmission lock-in technique, right) obtained by reflection lock-in technique

It is interesting to note that percentage errors are greatly reduced by carrying out the measurements in the transmission mode. Moreover the different behaviours between closer and farther defects from excitation source has a great influence on final results obtained in the reflection mode, because def. 17-18 phase trends show reference points in which it's possible to perform an estimation of discontinuities dimension; in opposition, in def. 16-19 trends, sharp peaks of phase are not visible, and this result in higher percentage errors.

4. Conclusions

This work analyzed the use of lock-in thermography for the estimation of simulated defects in thick glass-reinforced laminates used in the construction of luxury yachts. Different aspects were investigated: influence of defects aspect ratio, defects depth assessment, impact damage of the gel-coat layer.

The obtained results showed a good efficacy of optical excited lock-in thermography as a practical and contactless NDE tool, but also highlighted some limits related to the high transmittance coefficient of GFRP in the MWIR range.

As far as aspect ratio is concerned, a direct correlation between defect detection and this parameter was found, independently of actual defect depth.

The use of a transmission setup to carry out OLT measurements provided better results than conventional reflection setup for the identification of superficial impact damages.

REFERENCES

- [1] Pitarresi G., Licari A., Pasta A., "Thermal NDT of glass reinforced composites for naval applications by means of a linear infrared scanner", in Proc. 16th International Conference of Ship and Shipping Research, NAV2009, Messina, Nov. 25-27, 2009.
- [2] Sheppard P. J., Phillips H. J., Cooper I., "The practical use of NDE methods for the assessment of damaged marine composite structures", in Proc. of 17th International Conference on Composite Materials (ICCM 17), Edinburgh, UK, July 27-31, 2009.

- [3] Maldague X., Theory and practice of infrared technology for nondestructive testing, J. Wiley & Sons ed., New York, 684 p., 2001.
- [4] Meola C., Carlomagno G.M., Recent advances in the use of infrared thermography", Meas. Sci. Technol., vol. 15, pp. R27–R58, 2004.
- [5] Avdelidis N.P., Almond D.P., Dobbinson A., Hawtin B.C., Ibarra-Castanedo C., Maldague X., "Aircraft composites assessment by means of transient thermal NDT", Progress in Aerospace Sciences, vol. 40, pp. 143–162, 2004.
- [6] Sakagami T., Kubo S., "Applications of pulse heating thermography and lock-in thermography to quantitative nondestructive evaluations", Infrared Physics & Technology, vol. 43, pp. 211–218, 2002.
- [7] Carlomagno G.M., Berardi P.G., "Unsteady Thermo-topography in Non-Destructive Testing", III Infrared Information Exchange, pp. 33–40, St. Louis, Missouri, 1976.
- [8] Busse G., Rosencwaig A., "Subsurface imaging with photoacoustics", Appl. Phys. Lett., vol. 36, pp. 815–16, 1980.
- [9] Busse G., Wu D., Karpen W., "Thermal wave imaging with phase sensitive modulated thermography", J. Appl. Phys., vol. 71, pp. 3962–5, 1992.
- [10] Wu D., Busse G., "Lock-in thermography for nondestructive evaluation of materials", Rev. Gén. Therm., vol. 37, pp. 693–703, 1998.
- [11] Meola C., Carlomagno G.M., Squillace A., Giorleo G., "Non-destructive control of industrial materials by means of lock-in thermography", Meas. Sci. Technol., vol. 13, pp. 1583–1590, 2002.
- [12] Meola C., Carlomagno G.M., Giorleo L., "The use of infrared thermography for materials characterization", Journal of Materials Processing Technology, vol. 155–156, pp. 1132–1137, 2004.
- [13] Inagaki T., Ishii T., Iwamoto T., "On the NDT and E for the diagnosis of defects using infrared thermography", NDT&E International, vol. 32, pp. 247–257, 1999.
- [14] Choi M., Kang K., Park J., Kim W., Kim K., "Quantitative determination of a subsurface defect of reference specimen by lock-in infrared thermography", NDT&E International, vol. 41, pp. 119–124, 2008.
- [15] Karpen W., Wu D., Steegmuller R., Busse G., "Depth profiling of orientation in laminates with local lock-in thermography", QIRT 94, pp 281–286, Sorrento, Italy, 1994.
- [16] Gleiter A., Spießberger C., Busse G., "Phase angle thermography for depth resolved defect characterization", in Proc. 9th International Conference on Quantitative InfraRed Thermography (QIRT08), July 2-5, Krakow, Poland, 2008.
- [17] Maldague X., Marinetti S., "Pulse phase infrared thermography", J. Appl. Phys., vol. 79, pp. 2694–8, 1996.
- [18] Maldague X., Galmiche F., Ziadi A., "Advances in pulsed phase thermography", Infrared Physics & Technology, vol. 43, pp. 175–181, 2002.